


# Cu-Co/ZnAl<sub>2</sub>O<sub>4</sub> Catalysts for CO Conversion to Higher Alcohols Synthesized from Co-Precipitated Hydrotalcite Precursors

Benjamin Mockenhaupt<sup>1,4</sup>, Fatih Özcan<sup>2</sup>, Remco Dalebout<sup>3</sup>, Sebastian Mangelsen<sup>4</sup>, Thomas Machowski<sup>1</sup>, Petra E. de Jongh<sup>3</sup>, and Malte Behrens<sup>1,4,\*</sup>

DOI: 10.1002/cite.202200171

 This is an open access article under the terms of the Creative Commons Attribution License, which permits use, distribution and reproduction in any medium, provided the original work is properly cited.



Supporting Information  
available online

The role of Cu:Co composition in bi-metallic Cu-Co/ZnAl<sub>2</sub>O<sub>4</sub> catalysts on higher alcohol synthesis (HAS) was investigated at H<sub>2</sub>:CO = 4. The addition of Cu strongly facilitated Co reduction upon catalyst activation and suppressed coke deposition during HAS. Formation of predominantly hydrocarbons and higher alcohols was observed on the bi-metallic catalysts. Co/ZnAl<sub>2</sub>O<sub>4</sub> produced mainly CH<sub>4</sub> and Cu/ZnAl<sub>2</sub>O<sub>4</sub> mainly CH<sub>3</sub>OH, while at Cu:Co = 0.6 the best ethanol selectivity of 4.5 % was reached. The microstructure of the spent catalysts confirmed a close interaction of Cu and Co.

**Keywords:** Coking, Co-precipitation, Cu-Co bi-metallic catalysts, Higher alcohol synthesis, Zinc oxide

*Received:* August 29, 2022; *accepted:* September 08, 2022

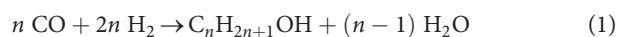
## 1 Introduction

Fischer-Tropsch synthesis (FTS) is an established process technology, based on reformed natural gas, with a high potential towards the reduction of the CO<sub>2</sub> footprint if bio-gas or CO<sub>2</sub>-reforming of natural gas are used as sources of synthesis gas [1, 2]. Advantages of this process lie in the possibility to tune the octane/cetane number of combustion fuels and to synthesize higher alcohols [3].

The FTS can be distinguished into the high temperature (300 °C–350 °C, ~30 bar) and the low-temperature processes (200 °C–250 °C, ~30 bar) [4–6]. For the low-temperature process Co-based catalysts are typically used, yielding long-chain hydrocarbons, which enables a further product upgrade by a cracking process [4, 7]. Methane and carbon dioxide, formed by the consecutive water-gas shift reaction, are low-value products and therefore undesired in the FTS process [4, 6]. In addition to synthetic fuel production, the higher alcohol synthesis (HAS) has received increasing attention, because such alcohols can be used as feedstock chemicals for several applications in the chemical industry [8].

Iron, cobalt and ruthenium are typical FTS-active metals. Because of the high price for ruthenium and the kinetic inhibition of iron by the coupled product water, cobalt seems to be a promising and cost-effective candidate also for HAS (Eq. (1)) [4, 6]. Further advantages of Co are the high activity in the low-temperature process as well as the stabil-

ity, but it usually exhibits a high selectivity to hydrocarbons, which is desired in conventional FTS, but not in HAS [4, 6]. To shift the product selectivity from hydrocarbons to higher alcohols, especially for carbon monoxide-rich synthesis gas, the combination of Co and Cu has been identified as promising [8].



According to a simplified picture of the current knowledge [2, 3, 9, 10], the dissociative adsorption of CO on a

<sup>1</sup>Benjamin Mockenhaupt, Thomas Machowski, Prof. Dr. Malte Behrens  
University of Duisburg-Essen, Inorganic Chemistry, Universitätsstraße 7, 45141 Essen, Germany.

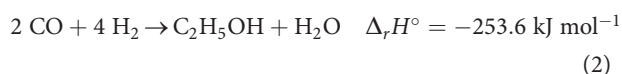
<sup>2</sup>Dr. Fatih Özcan  
University of Duisburg-Essen, Institute for Combustion and Gas Dynamics – Particle Science and Technology, Carl-Benz-Straße 199, 47057 Duisburg, Germany.

<sup>3</sup>Remco Dalebout, Prof. Dr. Petra E. de Jongh  
Utrecht University, Materials Chemistry and Catalysis, Universiteitsweg 99, 3584 CG Utrecht, Netherlands.

<sup>4</sup>Benjamin Mockenhaupt, Dr. Sebastian Mangelsen, Prof. Dr. Malte Behrens  
mbehrens@ac.uni-kiel.de  
University of Kiel, Inorganic Chemistry, Max-Eyth-Straße 2, 24118 Kiel, Germany.

cobalt surface enables a chain growth mechanism, which is important for long-chain products, but simultaneously increases possible catalyst inhibition by coke formation. Introducing Cu into a Co catalyst can increase the activity to alcohols, primarily to methanol, which is the major product on pure Cu catalysts, and iso-butanol because of the associative adsorption of CO and hydrogen spill over. Methane is a typical by-product as the optimum binding energies of the adsorbed intermediates in the methane and ethanol formation reactions are similar. Thus, methane formation will be hard to exclude in the HAS. Because of the higher exothermicity of the ethanol formation (Eq. (2)) and the higher molar reduction compared to methanation (Eq. (3)), low temperature and moderate pressure should thermodynamically favor the ethanol selectivity. Additionally, formed methanol can also act as an in situ synthesized carbon source, facilitating the formation of higher alcohols [11–13].

Ethanol:



Methane:



Theoretically, a Cu-Co alloy could balance the dissociative CO adsorption on the Cu-Co surface to enable chain growth and the associative adsorption of CO to enable conservation of the C–O bond [11, 12]. However, according to the phase diagram, Cu and Co do not form an alloy at temperatures below 600 °C [14], leading to segregation of the two metals. The controlled formation of alcohols instead of hydrocarbons with a cobalt-based catalyst thus poses a complex challenge and requires fine-tuning of the catalyst, its composition and microstructure [11]. It has been shown that nanosized alloy formation may occur during reduction, when Cu and Co are in close contact in a pre-catalyst phase, like in a CuCoMo catalyst [15] or in a CuCoAl catalyst derived from an ex-hydroxalcalite precursor phase [16].

An early study on alkali metal-promoted CuO/CoO/Cr<sub>2</sub>O<sub>3</sub> catalysts in HAS reported that pure copper catalysts produced methanol, whereas a Cu-rich Cu-Co/Cr<sub>2</sub>O<sub>3</sub> catalyst changed the selectivity to hydrocarbons or to higher alcohols, depending on the chromium concentrations. On Co-rich CuO/CoO/Cr<sub>2</sub>O<sub>3</sub> catalysts, rather the formation of hydrocarbons was favored [17]. These results already established the composition dependency of selectivity on a ternary catalyst component such as chromium. Addition of zinc is known to have an enormous effect on methanol synthesis on copper-based catalysts being able to tune the reactant selectivity between carbon monoxide and dioxide [18], but the presence of zinc in Cu-Co tri-metallic catalysts for HAS is not studied to an extent comparable to methanol synthesis. So far it is well understood that ZnO acts as a steric promoter preventing sintering and suppresses

methane formation due to intermediate stabilization in CuCoZnAl containing catalysts. Additionally, ZnO has a positive effect on the selectivity towards alcohols and limits/mitigates the cobalt carbide formation [19–22].

To enable the close contact between copper and cobalt, the incorporation of zinc, and at the same time the stabilization of the metallic phases in high dispersion thus avoiding deactivation by sintering effects, catalyst synthesis from a co-precipitated hydroxalcalite precursor phase is a suitable method as has been previously demonstrated for CuCoAl [16]. In such single-source precursors, the joint cationic lattice of divalent copper, cobalt and zinc in one crystalline hydroxalcalite phase enables the homogeneous distribution of the catalytically active species. In addition, a trivalent metal cation is needed to allow crystallization of the hydroxalcalite structure [23]. Using Al<sup>3+</sup> in a Zn:Al atomic ratio of 1:2 will formally give rise to a Cu-Co/ZnAl<sub>2</sub>O<sub>4</sub> composition of the resulting catalyst after calcination and reduction of the hydroxalcalite precursor. Aluminum as trivalent cation was previously discussed to enhance the catalyst performance due to the presence of stabilized Cu<sup>+</sup> species, which could be beneficial for the associative adsorption of CO [24]. The presence of basic sites, like surface OH groups or low coordinated O<sup>2-</sup> sites, in a CuCoAl catalyst is expected to lead to the formation of formate species, which could be an important intermediate for higher alcohols, as it is known from copper in methanol synthesis [11, 24–26]. Zinc promotes the formation of methanol from formate, which leads to the question whether the addition of zinc oxide to the Al<sub>2</sub>O<sub>3</sub> catalyst support (forming a ZnAl<sub>2</sub>O<sub>4</sub> spinel), can also promote the formation of higher alcohols.

To address these questions, the group of Muhler investigated a hydroxalcalite-derived catalyst series with systematically varied molar Cu:Co ratios from 1.4 to 3.6 and its catalytic performance in an equimolar H<sub>2</sub>:CO synthesis gas at 60 bar and 280 °C [10]. Copper enrichment resulted in a decreased conversion, but an increased selectivity towards methanol and ethanol and a moderate selectivity to hydrocarbons (below 50 % in total) [10]. In comparison, a zinc oxide-free catalyst has reached a higher CO conversion (36.2 % without Zn vs. 2.2 % with Zn) but accompanied by a simultaneously increased methane and methanol selectivity [10, 24].

In this study, we present a series of cobalt-rich Cu-Co/ZnAl<sub>2</sub>O<sub>4</sub> catalysts that have been synthesized by a co-precipitation of hydroxalcalite-based precursors and are compared to pure cobalt or copper reference catalysts. The performance of the catalysts has been investigated in the CO hydrogenation at lower pressure, decreased gas hourly space velocity (GHSV) and an increased hydrogen-to-carbon monoxide ratio compared to the study of Muhler and co-workers hypothesizing that these conditions could be beneficial for the higher alcohol yield on a zinc-promoted copper-cobalt catalyst [10, 24]. It was suggested that the enhanced catalyst-reactant contact time supports the chain growth resulting in heavier HAS products. The increased

water partial pressure could promote HAS by suppressing hydrocarbon formation and enable simultaneously the HAS via a formate mechanism by an in situ established water-gas shift cycle [27, 28]. In addition, our catalysts contained zinc and aluminum in a stoichiometric composition to form a stable spinel structure and thereby suppressing the incorporation of the catalytically active copper and cobalt species into a spinel structure. With such a  $\text{ZnAl}_2\text{O}_4$  support the zinc promotion compared to “free” zinc oxide will be moderated to mitigate the above-described dramatic breakdown of conversion, which may be related by active surface coverage with zinc species due to strong metal support interaction [29]. Finally, the hydrogen-enriched carbon monoxide synthesis gas was expected to avoid hydrogen becoming limiting and to suppress coke formation. This work addresses the effect of the Cu:Co ratio in such  $\text{ZnAl}_2\text{O}_4$ -supported catalysts on the selectivity and coking behavior in HAS.

## 2 Experimental Section

### 2.1 Catalyst Synthesis and Characterization

#### 2.1.1 Co-Precipitation of Hydrotalcite Precursors and Synthesis of Mixed Metal Oxides (MMOs)

The investigated precursor samples  $[(\text{Co}_{1-x}\text{Cu}_x)_7\text{ZnAl}_2(\text{OH})_6]\text{CO}_3 \cdot m \text{H}_2\text{O}$  with  $x = n_{\text{Cu}}/(n_{\text{Cu}}+n_{\text{Co}})$  were synthesized via co-precipitation according to Chakrapani et al. [30] in an automated stirred tank reactor (OptiMax 1001) from Mettler Toledo. Before co-precipitation was carried out, the reactor was filled with 200 mL deionized water and heated to 50 °C. The precipitation was carried out at a pH of 8.5 from a 0.4 M metal nitrate solution, prepared from metal nitrate salts with a purity  $\geq 98\%$  (see also Tab. S1 in the Supporting Information), under stirring (300 rpm) and with a dosing rate of  $2.08 \text{ g min}^{-1}$ . As precipitation agent a 0.6 M sodium hydroxide and 0.09 M sodium carbonate containing solution was used. After precipitation was performed, the ageing process started without any pH control at the same temperature (50 °C) for 1 h in the mother liquor. Afterwards, the precipitate was collected and washed several times with deionized water to remove excess ions until the conductivity of the washing water was less than  $100 \mu\text{S cm}^{-1}$  as measured with an immersion probe. The recovered powder was dried in a desiccator for three days under vacuum. Next, the dried precursor materials were calcined at 350 °C with a heating ramp of  $2 \text{ }^\circ\text{C min}^{-1}$  in static air in a muffle furnace. The temperature was held for 3 h.

#### 2.1.2 Characterization of Precursors, MMOs and Spent Catalysts

X-ray powder diffraction (XRPD) patterns of the calcined pre-catalysts and spent catalysts after CO hydrogenation

were recorded with  $\text{Mo-K}\alpha_1$  radiation on a Stadi-P from STOE, equipped with a Johansson-type germanium (111) monochromator and a MYTHEN 1 K detector. Line positions were calibrated against Silicon (NIST SRM 640d). The diffraction patterns were recorded at room temperature in the range of  $3^\circ$  to  $36^\circ 2\theta$ . The patterns of the precursors samples after co-precipitation were recorded on a Bruker D8 advance with  $\text{Cu-K}\alpha$  radiation and a LYNXEYE XE-T detector. The patterns were recorded in Bragg-Brentano geometry at room temperature between  $5^\circ$  and  $90^\circ 2\theta$ . Phase analysis was performed using structural data from ICSD and COD databases. Rietveld refinements [31] were carried out in TOPAS Academic [32] Version 6.0. The instrumental contributions to line broadening were determined via a Pawley fit [33] from a measurement of  $\text{LaB}_6$  (NIST SRM 660c) using a Thompson-Cox-Hastings profile. Microstructural effects leading to line broadening were modeled as an isotropic size effect and the volume average column height  $D_{\text{Vol}}$ . For the samples with larger amounts of hcp Co (in Cu-Co -catalysts compositions with  $x = 0$  and  $x = 0.125$ ) a simplified anisotropic model was used, which improved the fit significantly. Strain was omitted since this led to high correlations among the microstructure parameters. Due to this simplification the  $D_{\text{Vol}}$  should be regarded as apparent domain sizes that represents all microstructural effects. For the ccp metal the intensities especially for the 111 and 200 reflections differ significantly from those calculated for the bulk material due to stacking faults. Thus, stacking faults were modeled as implemented in TOPAS Academic V.6.0 [34], parameters were adjusted manually to achieve a reasonable fit.

Infrared spectroscopic characterization of the precursors and calcined samples was performed on a Bruker Alpha-Platinum Fourier-transform infrared (FT-IR) spectrophotometer with attenuate total reflection (ATR) unit. The spectra were recorded between  $400 \text{ cm}^{-1}$  and  $4000 \text{ cm}^{-1}$ . The spent samples after catalysis were analyzed on a Bruker Alpha-P ATR spectrophotometer. The recorded range was from  $100 \text{ cm}^{-1}$  to  $4000 \text{ cm}^{-1}$ .

Chemical composition of the spent catalysts was determined by C, H, N, S analysis in a Euro EA 3000 elemental analyzer from EuroVector. The combustion was performed in excess  $\text{O}_2$  at 1000 °C with He as carrier gas. The detection occurred in a thermal conduction cell.

Thermogravimetric analysis (TGA) was performed for the precursor materials on a STA 449 F3 Jupiter from Netzsch. The sample was heated by a heating rate of  $5 \text{ }^\circ\text{C min}^{-1}$  up to 1000 °C in synthetic air. The spent samples were analyzed in a STA 1600 from Linseis. The sample was heated up to 1000 °C in synthetic air by a heating ramp of  $4 \text{ }^\circ\text{C min}^{-1}$ .

Nitrogen physisorption was measured at 77 K in a Nova 3200e sorption station from Quantachrome and the data was analyzed by the method of Brunauer-Emmett-Teller (BET). Before recording the isotherms, the samples were degassed under vacuum at 80 °C (hydrotalcites) or 100 °C

(oxides) for 5 h. Afterwards the isothermal profiles between  $p/p_0 = 0.0$  and 1 were recorded. The multipoint BET surface area was determined by applying the BET equation in an individual range for each sample of  $p/p_0$  only considering the increasing volume by using the micropore BET assistant of the NovaWin software.

Temperature programmed reduction (TPR) of 30 mg of a 250–355  $\mu\text{m}$  sieve fraction of the calcined oxides was performed in a quartz glass U-shape tube reactor on a BelCat-B from Bel Japan Inc. First, the sample was dried by heating up with  $7^\circ\text{C min}^{-1}$  to  $100^\circ\text{C}$  in  $50\text{ mL min}^{-1}$  of pure Ar. The temperature was held for 60 min to ensure a complete drying of the sample. Afterwards, the temperature programmed reduction was performed. As reducing atmosphere, 6.4 vol%  $\text{H}_2$  in Ar with a volume flow of  $80\text{ mL}_\text{N}\text{min}^{-1}$  at ambient pressure was used. Starting from room temperature the sample was heated up to  $800^\circ\text{C}$  with a heating ramp of  $6^\circ\text{C min}^{-1}$ . After reaching the target temperature, it was held for 15 min to ensure a complete recording of the reduction profile. The formed water during reduction was separated by a mole sieve to enable the analysis of the consumed  $\text{H}_2$  via a thermal conductivity detector. The TPR profile of the pure copper sample was recorded using a BelCat II from Bel Japan Inc using 60 mg of a 250–355  $\mu\text{m}$  sieve fraction. The pretreatment and TPR recording were performed as described above. The hydrogen consumption was determined by thermal conductivity, which changes proportional to the consumed hydrogen.

### 2.1.3 Catalytic Testing

Catalytic testing of the synthesized mixed metal oxides was performed in a 16-fold parallel Flowrence plant of Avantium. Around 179 mg of a sieve fraction of 38–125  $\mu\text{m}$  was diluted with an equal amount of silicon carbide (SiC). The catalyst bed was placed in between a pre- and post-catalytic bed of SiC to ensure isothermal properties and to improve the warming up and mixing of the inlet gas stream. Before CO hydrogenation was performed, the catalytic materials were activated in pure hydrogen by heating up to with  $6^\circ\text{C min}^{-1}$  to  $120^\circ\text{C}$  under atmospheric pressure. The total volume flow was set to  $200\text{ mL}_\text{N}\text{min}^{-1}$  and divided for the individual reactors, meaning that each reactor of the 16-fold plant contained a partial volume flow of  $12.5\text{ mL}_\text{N}\text{min}^{-1}$ . After 30 min holding time, the temperature was increased up to  $250^\circ\text{C}$  with the same heating ramp. At this temperature, the reduction was performed for an additional 4 h to ensure a complete reduction of the catalyst. CO hydrogenation was performed using a hydrogen-to-carbon monoxide ratio of 4 and a total volume flow of  $75\text{ mL}_\text{N}\text{min}^{-1}$  resulting in a GHSV of around  $2800\text{ h}^{-1}$  per catalyst bed. The temperature was

varied from  $200^\circ\text{C}$  to  $300^\circ\text{C}$  in  $25^\circ\text{C}$  steps at a pressure of 20 bar. Afterwards, the initial temperature of  $200^\circ\text{C}$  was re-adjusted to evaluate the catalyst activity change in dependence of the temperature program. This step was followed by a second cycle of the same temperature program at a pressure of 60 bar without exposing the catalyst to ambient conditions. Each temperature step was held for 12 h to have enough time to take two gas chromatograph (GC) samples of each reactor.

To study the thermal stability of the catalysts, the maximum temperature was raised to  $380^\circ\text{C}$  and held for six hours. After this high-temperature treatment in synthesis gas, the catalysts were cooled back to  $200^\circ\text{C}$  to determine their activity change. This last process condition was held for 6 h. Afterwards, the catalyst beds were cooled down to room temperature in pure He. The catalysts were passivated by opening the reactor lid in a helium gas stream, to enable a smooth ventilation and slow air contact to re-oxidize the catalysts carefully. The data were evaluated by calculating the average of the two data points, representing the mean activity data over 6 h. The selectivities are based on the carbon balance and the whole data evaluation is described in detail in the Supporting Information (SI).

## 3 Results and Discussion

### 3.1 Catalyst Synthesis and Characterization

A catalyst series with varying copper-cobalt ratios as well as the pure cobalt and copper reference catalysts were synthesized by co-precipitation. The conditions of the co-precipitation were set to favor the formation of crystalline hydroxalcalite materials. The typical chemical formula of a hydroxalcalite mineral with carbonate ions in the interlayer can be as follows:  $[\text{M}^{2+}_8\text{M}^{3+}_2[(\text{OH})_{20}\text{CO}_3] \cdot m\text{H}_2\text{O}]$  with  $\text{M}^{2+}$  as divalent cations (Co, Cu and Zn) and  $\text{M}^{3+}$  as a trivalent cation (Al). In order to vary the metal ratios of the catalyst precursors, the composition was predefined by the metal salt solution and the nominal stoichiometric formula of the prepared precursors are listed in Tab. 1. The nominal

**Table 1.** Nominal metal composition of the co-precipitated cobalt-copper catalysts. The ratio of zinc to aluminum was chosen to be in the stoichiometric ratio of a spinel structure.  $x$  is the nominal fraction of copper based on the catalytic active metal (Co + Cu).

nominal Co, Cu fractions	$x_{\text{Cu}/(\text{Cu}+\text{Co})}$ , nominal	nominal precursor composition
0 % Co, 100 % Cu	1	$[\text{Cu}_7\text{ZnAl}_2(\text{OH})_{20}]\text{CO}_3 \cdot m\text{H}_2\text{O}$
50 % Co, 50 % Cu	0.5	$[\text{Co}_{3.5}\text{Cu}_{3.5}\text{ZnAl}_2(\text{OH})_{20}]\text{CO}_3 \cdot m\text{H}_2\text{O}$
62.5 % Co, 37.5 % Cu	0.375	$[\text{Co}_{4.375}\text{Cu}_{2.625}\text{ZnAl}_2(\text{OH})_{20}]\text{CO}_3 \cdot m\text{H}_2\text{O}$
75 % Co, 25 % Cu	0.25	$[\text{Co}_{5.25}\text{Cu}_{1.75}\text{ZnAl}_2(\text{OH})_{20}]\text{CO}_3 \cdot m\text{H}_2\text{O}$
87.5 % Co, 12.5 % Cu	0.125	$[\text{Co}_{6.125}\text{Cu}_{0.875}\text{ZnAl}_2(\text{OH})_{20}]\text{CO}_3 \cdot m\text{H}_2\text{O}$
100 % Co, 0 % Cu	0	$[\text{Co}_7\text{ZnAl}_2(\text{OH})_{20}]\text{CO}_3 \cdot m\text{H}_2\text{O}$

copper fraction of the catalytic active metals ( $x = n_{\text{Cu}} / (n_{\text{Cu}} + n_{\text{Co}})$ ) will be used as sample label for the precursors, calcined, reduced and spent catalysts.

The powders prepared via co-precipitation were analyzed by XRPD, the patterns are shown in Fig. 1a. The reflections can be assigned to the hydrotalcite structure without any additional reflections. This indicates crystalline phase purity and implies that a metal cation distribution close to the nominal composition is present in the hydrotalcite precursor, which enables a close contact in the resulting catalyst. Furthermore, with increasing copper content the 00l reflections (like  $2\theta = 11.6^\circ$  and  $2\theta = 23.4^\circ$ ) become much sharper, indicating an increased domain size (from 7 to 30 nm, see Fig. 1b), i.e., a larger number of stacked layers. From the severely broadened cross plane reflections 0kl (e.g., 012, 015, 018) substantial stacking disorder can be deduced, which is common in nanoscale layered materials. Since the only observed reflection with  $l = 0$ , which is 110, is of low intensity, no reasonable information on the in-plane domain size is available. The lattice parameters evolve according to the change in chemical composition. While  $a$  shows a near constant value of 3.09 Å for  $x = 0$ –0.5 it drops to 3.05 Å for  $x = 1$ . Even more sensitive is  $c$ , which drops from 23.28 Å to 22.53 Å when substituting  $\text{Co}^{2+}$  for  $\text{Cu}^{2+}$  in a near

linear way. The significant contraction of the unit cell along this axis cannot be explained by the rather similar ionic radii (75 and 73 pm, respectively) and may indicate a decrease in water content in the interlayer space, which would be a viable explanation.

IR spectroscopy (shown and discussed in the SI, Fig. S1a) shows spectra expected for hydrotalcite materials and support the above-described hypothesis by the decreasing water deformation mode and the additional weaker hydroxyl stretching mode by increasing copper content. The calcinations to the corresponding MMOs were performed at 350 °C in an analogous way as it is known for copper-based methanol synthesis catalysts [35]. This temperature leads to decomposition of the hydrotalcite structure but does not cause a complete decomposition of the carbonate species. It rather leads to a remainder of so-called high-temperature carbonate, which is discussed to mitigate metal oxide sintering and results in a more nanostructured catalyst [36]. This was also confirmed for our copper-rich samples by thermogravimetric analysis of all prepared precursors (shown and discussed in Fig. S2). The XRPD patterns of the MMOs shown in Fig. 1c confirm the complete decomposition of the precursor phase. On the Co-rich side, the formation of a spinel phase is evident with a lattice parameter of  $a = 8.08$  Å

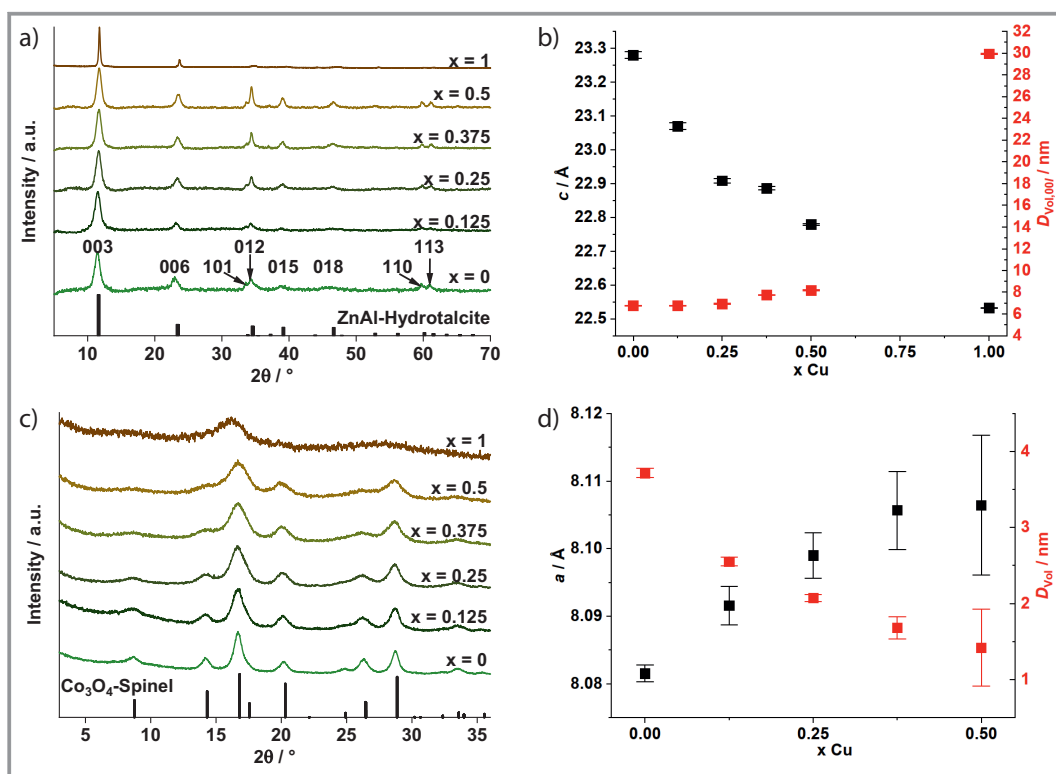


**Figure 1.** Powder XRD pattern of the co-precipitated  $[(\text{Co}_{1-x}\text{Cu}_x)_7\text{ZnAl}_2(\text{OH})_{20}]\text{CO}_3 \cdot m \text{H}_2\text{O}$  hydrotalcite precursors (a) with  $x = n_{\text{Cu}} / (n_{\text{Cu}} + n_{\text{Co}})$ . The reference was taken from the ICSD database for a Zn-Al-Hydrotalcite (ICSD#155052). The reflections are labeled with the corresponding Miller indices taken from the reference. In b) the variation of the lattice parameter  $c$  and domain size along the  $c$ -axis is plotted as function of chemical composition. c) XRPD patterns of the mixed metal oxides after calcination at 350 °C in static air of the corresponding hydrotalcite precursor. The reference of  $\text{Co}_3\text{O}_4$ -spinel was taken from ICSD database (ICSD#26091). The extracted lattice parameter  $a$  and isotropic domain size are plotted in d).

(Fig. 1d). The broad reflections were refined as isotropic domain size with  $D_{\text{Vol}} = 3.7(5)$  nm. However, it should be noted that a discrimination among different spinel phases (e.g.,  $\text{ZnAl}_2\text{O}_4$  and  $\text{Co}_3\text{O}_4$  or a mixed phase) is not possible given the similar lattice parameters and the broad reflections. Thus, the values can only be understood as the sample average. Still a trend can be deduced, with increasing Cu content up to  $x = 0.5$  the domain size decreases down to  $1.5(5)$  nm and  $a$  increases slightly to  $8.1(1)$  Å. For  $x = 1$  the sample can be regarded as amorphous since only one broad halo is visible.

Interestingly, the pure cobalt sample ( $x = 0$ ) has the highest specific surface area after calcination, shown in Fig. S5. The accessible surface areas of the precursors were in the same range around  $80 \text{ m}^2\text{g}^{-1}$ , except for the pure copper containing ( $x = 1$ ) hydrotalcite reaching only roughly half of that value. The increase in surface area due to the calcination is attributed to the released water and carbonates leading to pore formation in the materials. Additionally, the temperature was low enough to avoid metal oxide sintering yielding a porous material [36]. The oxide surface areas of the copper-rich MMOs ( $x = 0.25$ – $0.50$ ) were similar and reached values around  $100 \text{ m}^2\text{g}^{-1}$ . Contrarily, the cobalt-rich samples ( $x = 0$ – $0.125$ ) reached even higher surface areas above  $160 \text{ m}^2\text{g}^{-1}$  showing that large specific surface areas of the MMO pre-catalysts can be achieved for the more crystalline samples (Fig. 1c) that do not contain high-temperature carbonate.

The TPR results of the catalyst series are shown in Fig. 2. The temperature labels refer to the temperature of highest rate of hydrogen consumption. The cobalt-free sample ( $x = 1$ ) shows a slight increase in the hydrogen consumption signal starting at  $\approx 200$  °C and reaching the maximum rate at about 334 °C. Afterwards, an additional broad signal was observed around 537 °C. These two temperature ranges indicate that there are two different reducible species present in that sample. The one at lower temperature is assigned to copper oxide being reduced to copper metal, while the

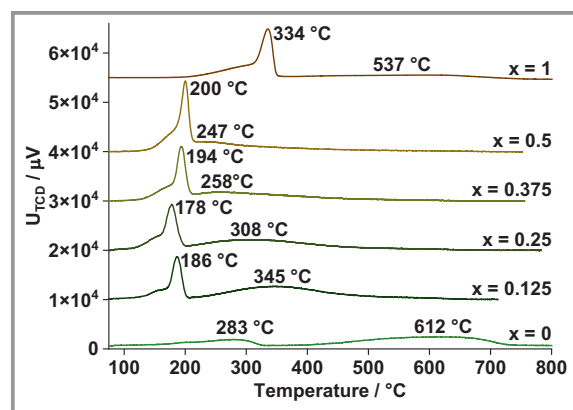


**Figure 2.** TPR profiles of a sieve fraction of 250–355  $\mu\text{m}$  of the prepared pre-catalysts. The reduction was measured in 6 vol %  $\text{H}_2$  in Ar with a heating rate of  $6 \text{ }^\circ\text{C min}^{-1}$ . The labeled temperatures indicate the maximum hydrogen consumption.

one at higher temperature can be attributed to zinc oxide reduction and brass formation [37]. A similar behavior was observed for the pure cobalt sample ( $x = 0$ ), where the low-temperature reaction is assigned to  $\text{Co}_3\text{O}_4$  reduction to CoO and the high-temperature peak to formation of cobalt metal as discussed in detail in the SI.

The TPR analysis of the binary Cu-Co samples demonstrates that the copper reduction is lowered gradually to 180 °C with increasing amounts of cobalt. The typical shape of the CuO reduction with a shoulder assigned to intermediate Cu(I) formation [38, 39] remained unaltered. Additionally, a second broad peak was observed at temperatures higher than the CuO reduction peak and was found to increase with the cobalt content in the Cu-Co samples. This additional peak was similar in shape to the second reduction process observed in the pure cobalt or copper sample at higher temperature and was not followed by any other reduction peak upon further heating. As the formation of brass was not observed in hydrotalcite-derived copper catalysts at these low temperatures [38, 39], this broad peak is tentatively assigned to the cobalt metal formation shifted by the presence of metallic copper to lower temperatures compared to the pure cobalt reference. This effect is likely caused by spillover of activated hydrogen from the freshly formed copper metal particles. With lowering cobalt content, this second feature can be shifted down in temperature to 247 °C for the equimolar sample ( $x = 0.5$ ), in comparison to 612 °C in the pure cobalt sample ( $x = 0$ , Fig. 2). A small amount of copper ( $x = 0.125$ ) does already facilitate the reduction of cobalt oxide, but the maximum hydrogen uptake at high temperature is shifted only to 345 °C. These findings suggest that after the activation of the catalysts at 250 °C with pure hydrogen, only the copper-rich binary catalyst  $x = 0.5$  can be safely expected to contain fully reduced copper and cobalt species before CO hydrogenation started. Thus, this catalyst will be discussed in more detail below as a representative of the bi-metallic samples.

### 3.2 Activity Test in CO Hydrogenation

The reference temperature of the CO hydrogenation was chosen to be 200 °C to remain in the kinetic regime preventing thermodynamic limitations. The binary Cu-Co catalysts performed in a similar manner in the catalytic activity tests.  $\text{C}_{5+}$  products were sometimes present but only as a very minor fraction. Therefore, the discussion of the catalyst's composition-dependent activity and selectivity will be conducted in the following for three selected  $\text{ZnAl}_2\text{O}_4$ -supported catalysts, the pure Co- ( $x = 0$ ), the pure Cu- ( $x = 1$ ) and the binary catalyst with an equal molar ratio Cu:Co = 1 ( $x = 0.5$ ) based on the selectivity for linear  $\text{C}_1$  to  $\text{C}_4$  products. The conversions and selectivities of all investigated Cu-Co catalysts are shown and discussed in the SI Fig. S7–S11. The process parameters over the time on stream of the catalytic test are also provided in Fig. S6.

### 3.2.1 CO Hydrogenation at 20 bar

After activation in pure hydrogen at 250 °C for 4 h, the pure Co and Cu catalysts reached low CO conversions at 200 °C and 20 bar as shown in Fig. 3a. Generally, low conversion was expected for Cu catalysts compared to Co. Based on the TPR profiles (Fig. 2), the reduction temperature of 250 °C likely resulted in an incomplete reduction of these MMOs giving rise to the low activities for both catalysts. The high CO<sub>2</sub> content in the product gas stream (shown in Fig. S9a) indicated on-going reduction and supports this assumption. The pure cobalt and copper catalysts formed only low amounts of hydrocarbons or long chain alcohols (Fig. 3b,c) from which the water molecule could be reconsumed by water-gas-shift reaction to form CO<sub>2</sub>. Therefore, the CO<sub>2</sub> selectivity rather indicates on-going reduction of the MMOs.

The binary Cu-Co ( $x = 0.5$ ) catalyst showed higher conversion and selectivity to hydrocarbons and the increase in reaction temperature by 25 °C further enhanced the activity of Cu, Co and CuCo catalysts but also the hydrocarbon

selectivity. Traces of ethanol was formed for the pure Co catalyst ( $x = 0$ ) at 225 °C (Fig. 3c). The binary Cu-Co ( $x = 0.5$ ) catalyst formed alcohols, but less with lower selectivity level than at 200 °C. On the pure Cu catalyst ( $x = 1$ ), the product distribution shifted towards methanol with increasing temperature with a simultaneous selectivity of around 10% for C<sub>1</sub> to C<sub>4</sub> hydrocarbons. Because of this hydrocarbon formation with water as a by-product, the selectivity of CO<sub>2</sub> was for this catalyst almost constant over the temperature range and is assigned to the water gas shift reaction.

Temperatures of 250 °C–300 °C at 20 bar resulted in complete CO conversion for all cobalt-containing catalysts (cf. SI Fig. S7). Thus, the catalytic performance will be discussed only in the kinetic region at 200–225 °C. The datapoint at 200 °C before the catalyst has been exposed to harsher catalytic conditions (250 °C–300 °C) will be compared to the datapoint after returning back to 200 °C in temperature program (cf. process scheme in Fig. S6) as a rough measure of catalyst stability. Back at 200 °C (after T-variation in Fig. 3), the activity was enhanced, compared

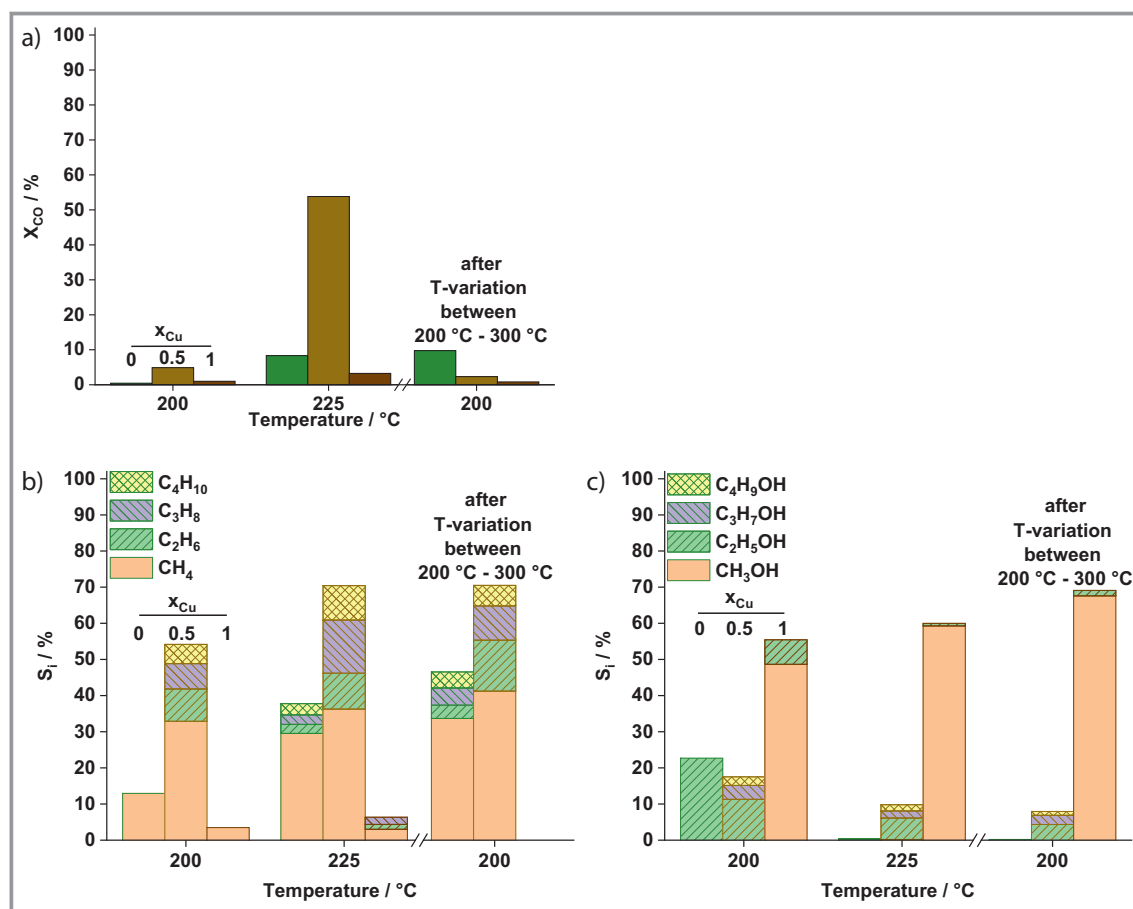


**Figure 3.** In a) the CO conversion of selected catalysts and temperatures ( $x = 0$  (left bar),  $x = 0.5$  and  $x = 1$  (right bar)) at 20 bar are shown. Below are the corresponding selectivities and product distribution ( $n$ -C<sub>1</sub> to  $n$ -C<sub>4</sub>) in the b) alkane- and c) alcohol formation presented. The second run at 200 °C was performed after the temperature variation ( $T$ -variation) to reference activity changes due to catalyst ageing. The total volume flow was set to 75 mL<sub>N</sub>min<sup>-1</sup> with H<sub>2</sub>:CO = 4 and GHSV = 2800 h<sup>-1</sup>.

to the initial catalytic performance at 200 °C, for the pure Co catalyst and slightly lowered for the mixed Cu-Co catalyst ( $x = 0.5$ ) but almost equal for the copper catalyst, which formed, as expected, mainly methanol with only a small amount of ethanol (cf. SI Fig. S7b,c). The increase in the activity of the Co catalyst ( $x = 0$ ) can be attributed to a more complete reduction under high pressure in a strongly reducing  $H_2/CO$  atmosphere which might compensate the need for higher temperature as it was expected from TPR results (Fig. 2). Simultaneously, the hydrocarbon selectivity increased, with predominantly methane being formed, and the selectivity towards ethanol completely vanished, as expected for a pure cobalt catalyst [19]. The initial ethanol formation (at low conversion) thus was not stable and cannot be assigned to the effect of zinc on the cobalt catalyst but rather to the still oxidized nature of the catalyst after incomplete activation.

Stable  $C_2$  to  $C_4$  alcohol formation at 200 °C was observed only over the Cu-Co mixed catalysts. This selectivity is ascribed to the interplay between both metals and confirms

the promotional effect of bi-metallic catalysts explained by theory [11] and reported in the literature [10, 16]. Interestingly, as shown in the SI Fig. S7, already a relatively low amount of copper (12.5 at% Cu in the catalyst with  $x = 0.125$ ) in the cobalt catalyst resulted in an increase of the ethanol selectivity from 0.3 % to 4 % at 200 °C and 20 bar after the temperature treatment. The best catalyst at these conditions, was a cobalt-rich binary sample with  $x = 0.375$  with an ethanol selectivity of 4.5 % (shown in the SI Fig. S7c and Fig. S10).

### 3.2.2 CO Hydrogenation at 60 bar

The increase of the pressure from 20 to 60 bar favors the CO conversion as is expected for a reaction with volume contraction such as HAS (Eq. (1)). The CO conversion of the pure Co catalyst ( $x = 0$ ) increased with increasing pressure roughly by factor of three (compare Fig. 3, second run (after T-variation) at 200 °C with Fig. 4, first run at 200 °C). However, the conversion increased only slightly for the

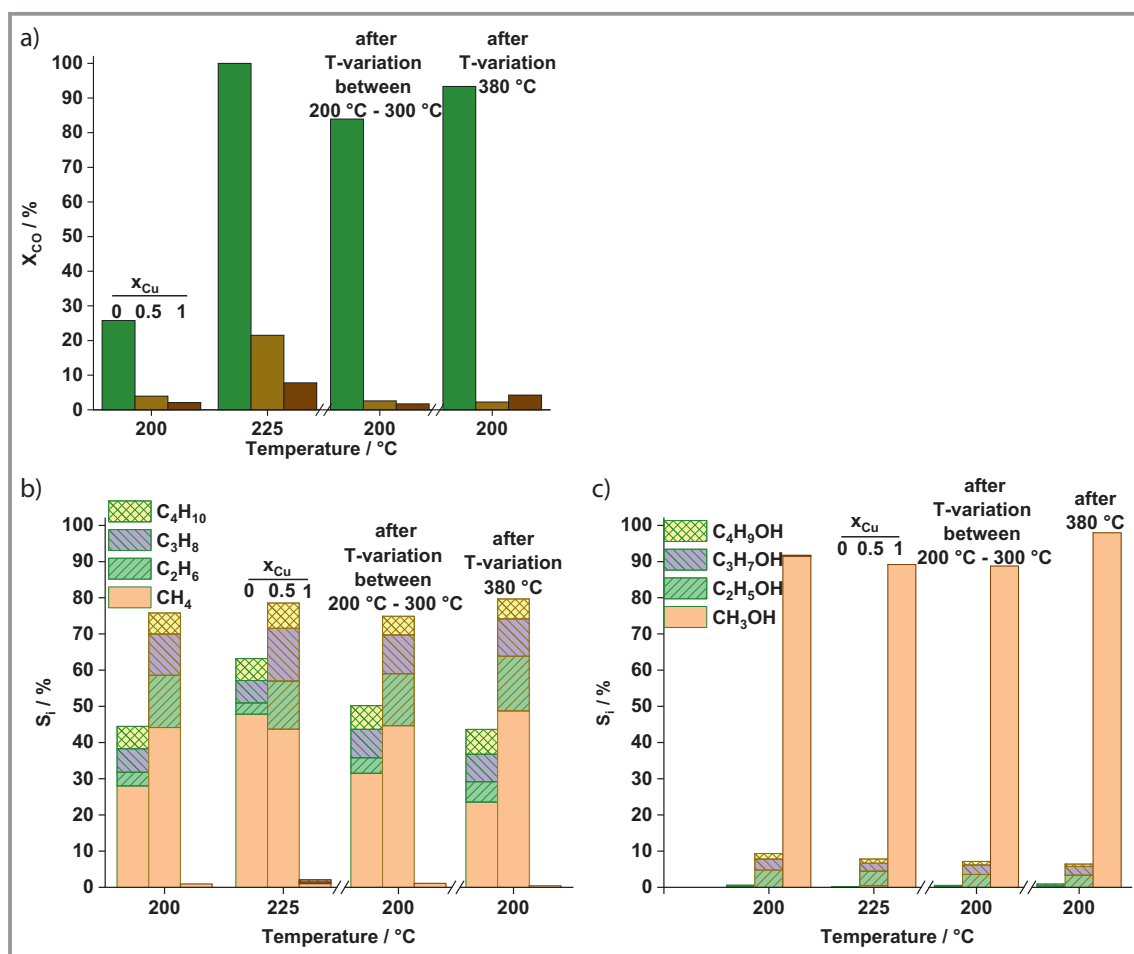


**Figure 4.** a) CO conversion of selected catalysts ( $x = 0$  (left bar),  $x = 0.5$  and  $x = 1$  (right bar)) at 60 bar. Below are the corresponding selectivities and product distribution ( $n-C_1$  to  $n-C_4$ ) in the b) alkane- and c) alcohol formation presented. The second run at 200 °C was performed after the temperature variation (T-variation) to reference activity changes due to catalyst ageing. The third run at 200 °C was performed after 380 °C to reference activity changes due to possible sintering effects. The total volume flow was set to  $75 \text{ mL}_N \text{ min}^{-1}$  with  $H_2:CO = 4$ .



copper-containing catalysts. The observed formation of the  $C_1$ - $C_4$  alcohols at low temperatures ( $< 250^\circ\text{C}$ ) and the formation of hydrocarbons with increasing temperature ( $> 225^\circ\text{C}$ ) agrees with theory [12]. In our study, the product distribution remained similar for all catalysts, only the overall selectivity was increased. Also, the reference run at  $200^\circ\text{C}$  at 60 bar (Fig. 4,  $200^\circ\text{C}$ , after T-variation) did not show any strong change of the CO conversion or the selectivity of the copper-containing samples in comparison to the previous catalytic test at  $200^\circ\text{C}$ , indicating a stable performance and product distribution.

In comparison with reported results on similar catalysts, our ethanol selectivities are modest (Fig. 4c). The herein reported copper-cobalt catalyst with equimolar ratio ( $x = 0.5$ ) reached a selectivity to ethanol of 2.5 % at a full conversion at 60 bar and  $250^\circ\text{C}$  whereas a similar catalyst prepared in the group of Muhler reached a selectivity of 7.5 % at a conversion of 9.3 % at 60 bar, a higher *GHSV* around  $9600\text{ h}^{-1}$  and  $280^\circ\text{C}$  [10]. In the herein presented study, no ethanol formation was observed at a temperature around  $250^\circ\text{C}$  for our self-prepared Cu-Co catalyst ( $x = 0.5$ , *GHSV*  $\approx 2800\text{ h}^{-1}$ , full conversion). The main differences between literature catalytic performance and this study are the lower reaction temperature and the higher hydrogen excess in the herein described experiments ( $\text{H}_2:\text{CO} = 4$  vs  $\text{H}_2:\text{CO} = 1$ ) [10], which is a composition closer to methanation stoichiometry than to ethanol formation. An additional difference is the copper content, which was  $x = 0.6$  of the above-mentioned literature reference [10] and  $x = 0.5$  for the herein reported catalyst.

The CO conversion on the pure cobalt catalyst ( $x = 0$ ) kept changing at the different reference measurements over the complete catalysis run of 165 h at varying conditions, also in the experiments conducted at 60 bar. The CO conversion changed from 26 % to 84 % during the temperature variation in between of the two measurements at  $200^\circ\text{C}$  of the first and second run (Fig. 4). The main products were hydrocarbons. This activity increase must be related to some structural changes of the pure cobalt catalyst ( $x = 0$ ). The absence of  $\text{CO}_2$  formation during the temperature treatment (SI, Fig. S9b) does in this case exclude a reduction of cobalt oxide residues as it was suggested in the catalytic tests at 20 bar. It further indicates that a steady extent of reduction has been reached without any water gas shift (WGS) activity. A promotion of zinc oxide in a similar manner as it is known from copper-methanol catalysts was not observed for cobalt catalysts, but a stabilizing effect was reported covering the catalyst activity [19]. Therefore, the increase in conversion of the pure cobalt catalyst must be caused by a structural rearrangement of the activated cobalt species.

During the following thermal stability test at  $380^\circ\text{C}$  still further improvement of the CO conversion to 93 % was observed after returning to kinetic control at  $200^\circ\text{C}$  (see Fig. 4 and SI Fig. S8). Again, at the  $380^\circ\text{C}$  test no  $\text{CO}_2$  formation was observed. The high selectivity of hydrocarbons and the

absence of alcohols (cf. SI Fig. S8b,c) lead more to the conclusion, that probably the products have changed the active site of the cobalt catalyst. Since it is known that cobalt forms cobalt carbide at higher temperatures, the carburization would be noticed by a lowered CO conversion, which was not the case in our catalytic tests [40]. On the other hand, a change of the cobalt phase induced by hydrocarbon deposition and hydrogenation could have activated the cobalt catalyst by forming a more active hcp cobalt site, which was to some extent found in the spent sample (cf. Fig. 5b). [41]

A slightly increased CO conversion over the pure Cu catalyst ( $x = 1$ ) from 2 % at  $200^\circ\text{C}$  before  $380^\circ\text{C}$  and 60 bar (Fig. 4a) to 4 % at  $200^\circ\text{C}$  after  $380^\circ\text{C}$  and 60 bar and an increased  $\text{CO}_2$  selectivity during CO hydrogenation at  $380^\circ\text{C}$  (Fig. S9b) were observed and may indicate an on-going activation process of this catalyst beside the WGS activity as it was observed over the complete temperature range. Simultaneously, the selectivity of methanol increased by 10 % from 89 % to 99 %. This behavior might be explained by enhanced strong metal-support interaction as the  $\text{ZnAl}_2\text{O}_4$  support starts to reduce at higher temperatures in accordance with the hypothesis that a Cu-Zn surface alloy can favor methanol synthesis [37, 42]. Also, on-going sintering can lead to a gradual activity increase of supported Cu catalysts [43].

In summary, it was shown that the cobalt catalyst ( $x = 0$ ) changed the active site during reaction after reaching full activation and that for the hydrotalcite-derived copper catalyst ( $x = 1$ ), the CO conversion and methanol selectivity increased after developing a highly active site at high temperature treatment. However, subsequent activation played a much smaller role for the bi-metallic catalysts due to strongly lowered reduction temperatures of these samples.

Instead, the CO conversion of the mixed Cu-Co catalysts decreased only slightly over 63 h of time (SI Fig. S8 and Fig. S6) during the temperature variation test up to  $300^\circ\text{C}$  at 60 bar, likely due to particle growth caused by the strongly reducing atmosphere and the relatively high temperature that, according to the TPR profiles (Fig. 2), should lead to a full reduction. Their performance in the run at  $200^\circ\text{C}$  and 60 bar resulted in a relatively unaffected selectivity towards alcohols from  $C_2$  to  $C_4$  (SI Fig. S8c) demonstrating again that the catalysts are quite stable in product formation at these strongly reducing conditions upon temperature and pressure variations. Up to the last reference experiment at  $200^\circ\text{C}$  at 60 bar, the catalysts reached 150 h on stream before the thermal stability test at  $380^\circ\text{C}$  was performed.

During the high temperature catalysis at  $380^\circ\text{C}$ , the binary catalysts reached full conversion and formed only hydrocarbons (cf. SI Fig. S8). Their catalytic performance in CO conversion was reduced by half comparing the kinetic experiments at  $200^\circ\text{C}$  of the initial run and after  $380^\circ\text{C}$ . The maximum activity loss of 55 % was observed for a cobalt-rich catalyst ( $x = 0.25$ ). This activity loss

could be caused by metal sintering or coking. However, the selectivities were unaffected by the temperature treatment.

### 3.3 Characterization of the Spent Catalysts after Passivation in Air

To better understand the state of the catalysts and especially the above-described dynamic changes of the copper-free Co catalyst ( $x = 0$ ), the spent samples were analyzed after careful air contact as described in the experimental section. The XRPD patterns of the spent catalysts are presented in Fig. 5a. They were all analyzed with Rietveld refinement to extract the lattice parameters and the quantitative composition of the assigned phases (shown in SI Fig. S15). Due to a partial overlap of reflections and correlation with the background, the estimated error in the quantification was 1–2 % and the microstructure was treated only in a simplified manner without distinguishing size and strain effects to not overparametrize the fits. Because both copper and cobalt

can crystallize in the ccp structure with similar lattice parameters only one ccp phase was modeled. For the ccp metal, a model for stacking faults was included to account for the resulting altered intensities, which are well known to occur in this material [44].

All samples contain a spinel phase after catalytic treatment up to 380 °C, which is assigned to the  $\text{ZnAl}_2\text{O}_4$  support. It accounts in all samples for  $\sim 40$  wt % (see Fig. 5b) of the sample and a significant inversion between  $\text{Zn}^{2+}$  and  $\text{Al}^{3+}$  across their sites of  $\sim 30$  % was found. The expected weight fraction of the  $\text{ZnAl}_2\text{O}_4$  in a fully reduced catalyst with composition  $\text{Cu}_7\text{ZnAl}_2\text{O}_4$  (cf. composition of the precursor) would be  $\sim 30$  %. This overestimation of the weight fraction by  $\sim 10$  % may in part due to errors in the quantification but may as well indicate amorphous content in the sample.

There is a significant change in lattice parameter of the spinel phase with chemical composition of the catalysts, in particular a shrinkage of the cell parameter  $a$  with increasing Cu content (Fig. 5c). The domain size shows a minimum at around  $x = 0.25$ – $0.375$ , which indicates either a

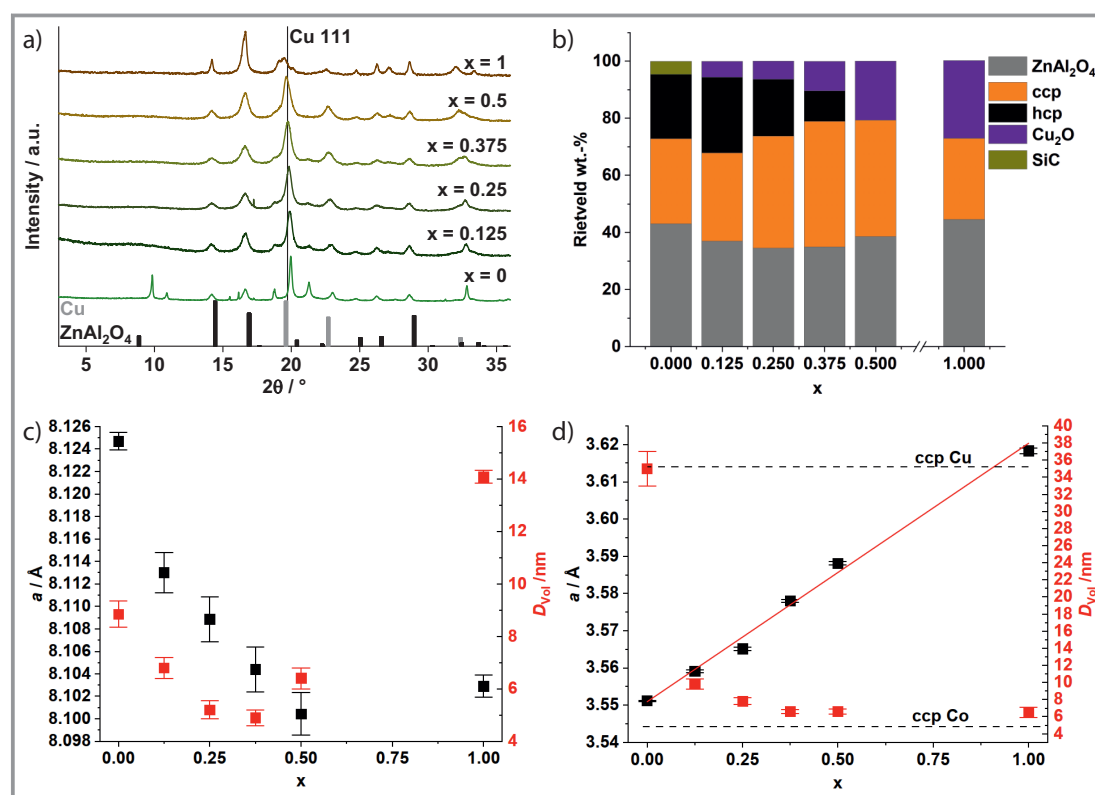


**Figure 5.** Powder XRD analysis of the spent catalysts after CO hydrogenation at 20 bar / 60 bar and 200 °C–380 °C after passivation at room temperature with air. The complete pattern as visualized in a) with the dark grey bars corresponding to the Cu (ccp) reference (ICSD#7954) and the black bars corresponding to the  $\text{ZnAl}_2\text{O}_4$  reference (ICSD#609005). The resulting quantification of the assigned phases by a Rietveld refinement is shown in b). c) Compositional dependence of the cell parameter and domain size of the spinel phase. d) The ccp phase shows a significant expansion of the cell parameter with the copper content  $x$ . The red line is a linear fit to all data points, the dashed lines indicate the lattice parameters for bulk ccp Cu and Co taken from several entries of the ICSD (#627115, 627114, 622435, 44989). The apparent domain size shows a drastic initial decrease upon addition of copper in the catalyst system.

smaller crystallite size or could also be caused by substitution. A substitution of  $\text{Zn}^{2+}$  by  $\text{Co}^{2+}$  seems to be a likely case [45], which would render the spinel support at least chemically active in an interaction with the catalyst.

In addition to the spinel phase, metallic phases are present in all samples. For the copper-rich samples with  $x = 1$  and 0.5 only ccp metal was found, while for lower values of  $x$  a coexistence of ccp and hcp metal was observed (Fig. 5b). The sample with  $x = 0$ , i.e., only cobalt as catalyst, needs special attention here: Firstly, the coexistence of a hcp and ccp metal phase suggests that cobalt adopts both polymorphs here. The thermodynamically stable form is hcp, both at room temperature and even at the highest catalyst test temperature (380 °C). The coexistence of both polymorphs in various specimen and the complex dependency on heat treatment and particle size is long known [46]. However, alloying with other metals (e.g., Zn) could contribute to further stabilizing (partially) the ccp phase, since a Co-rich alloy with Zn adopts the ccp structure [47]. The lattice parameters of both phases are well in agreement with those reported in literature for hcp and ccp Co [48]. Secondly, the metal phases show a much higher crystallinity in the pure cobalt catalyst ( $x = 0$ , Fig. 5a) as compared to all other compositions. As soon as copper is introduced the domain size of the metal phases decreases substantially from 35 nm for  $x = 0$  to 6.5 nm for  $x = 1$  (see Fig. 5d), where the most significant drop down to 10 nm already occurs with a small addition of copper, i.e., for  $x = 0.125$ . It should be noted that these domain sizes rather underestimate the actual domain size, in particular since no strain was modeled for the sake of stabilizing the fit. But strain is expected due to the well-known defective nature of ccp metal nanoparticles. The actual metal particle size will be underestimated even by a higher extent as these may consist of several domains. Furthermore, the formation of  $\text{Cu}_2\text{O}$  due to passivation will also reduce the average domain size of the ccp phase since the oxide will grow at the expense of the metal.

When tracing the evolution of the cell parameter of the ccp phase (see Fig. 5d) with chemical composition of the catalyst a virtually linear trend is evident suggesting alloying of Cu and Co. This is surprising since no miscibility between Cu and Co is known in the bulk. The difference plots do not indicate the need for additional phases to fit the patterns and favor such single metal phase scenario. Still, one should bear in mind that two coexisting ccp phases may cause such linear change in apparent cell parameter by a constant shift of their phase fractions as an alternative scenario. Given the similar lattice parameters, severe line broadening and limited angular range it is virtually impossible to discriminate among the two scenarios.

However, the situation is even more complex if we consider the presence of reduced zinc in the catalysts, according to the Cu/ZnO methanol catalyst [37, 42], there is a reasonable possibility that cobalt and zinc form mixed particles or a surface alloy with a cobalt-rich core under reaction condi-

tions in a ccp phase [49], which can be undetected by XPRD as in the case of Cu/ZnO. Additionally, it can be discussed that the Cu-Co mixed phase creates a CuCo surface alloy representing multiple weak CO adsorption sites lowering the C–O dissociation and increasing the selectivity towards oxygenated FTS products [50]. The nanostructure of the catalyst could enhance the number of such CuCo surface alloy enhancing the alcohol formation. In this scenario, depending on the reaction conditions, the yield of alcohols can be seen as an indicator of such a Cu-Co mixed phase whereas the hydrocarbon formation refers to the fraction of active pure Co surface. Alternatively, methanol formation on (pure) Cu was discussed, which could promote HAS by in situ formed methanol [11].

Additionally, all copper containing samples contain a detectable amount of  $\text{Cu}_2\text{O}$  that increases with  $x$  (Fig. 5b), which results likely from the treatment of the catalysts in air after the experiments. It should be noted that CoO may have formed as well, as the two compounds  $\text{Cu}_2\text{O}$  and CoO show very similar diffraction patterns. Given the broad reflections a distinction is not possible. For the sample containing only cobalt, the formation of significant amounts of crystalline CoO is not evident, which implies a quantitative reduction of the oxidic (spinel) precatalyst under reaction conditions. Furthermore, this sample contains minor amounts of SiC, which was used as diluent for the catalyst during activity tests. This sample is also unique in showing two additional reflections at 9.8 and 10.9°  $2\theta$ , which remain unassigned after searching the databases. Based on IR and TGA results (see SI Fig. S12–S14) they are tentatively assigned to crystalline fractions of hydrocarbon waxes or other carbonaceous deposits [51].

The formation of cobalt carbide and graphitic hydrocarbons was observed previously on Cu-Co catalysts with different cobalt-to-copper ratios [52]. Formation of cobalt carbide was not observed in the XRPD patterns of the spent samples (Fig. 5a) since no corresponding additional reflections could be observed. This leads to the conclusion that bulk cobalt carbide could only be present as a minor phase or in an amorphous state if present at all. Surface carbide is expected to lower hydrocarbon selectivity and enhance the formation of alcohols because of the enhanced associative adsorption of CO. Simultaneously, the carbide formation results in a deactivation of the catalytic performance, which was observed before to stabilize only after 40 h time on stream [52, 53]. Such a behavior was not found in this study supporting the absence of cobalt carbides in these Cu-Co/ $\text{ZnAl}_2\text{O}_4$  catalysts at the applied reaction conditions.

IR spectroscopy of the spent samples (see Fig. S12) shows for the copper-containing catalysts absorption bands between 1541  $\text{cm}^{-1}$  and 1393  $\text{cm}^{-1}$ , which probably correspond to carbonate stretching modes, similar as in the calcined catalysts. However, unlike there, this carbonate is not necessary a residue of the synthesis, but rather additional surface carbonate formed from  $\text{CO}_2$ . Only for the pure cobalt catalyst with  $x = 0$ , strong absorption bands around 3000  $\text{cm}^{-1}$

and  $1500\text{ cm}^{-1}$  were observed. These strong bands at  $1474\text{ cm}^{-1}$  and  $1460\text{ cm}^{-1}$  can be assigned to methyl groups of formed coke or aliphatic hydrocarbons. Asymmetric C–H bending can give rise to the band at wavenumber  $1460\text{ cm}^{-1}$  [54,55]. In the range of  $3000\text{ cm}^{-1}$  and  $2800\text{ cm}^{-1}$ , C–H stretching modes are excited [55]. The band at  $2953\text{ cm}^{-1}$  could be assigned to asymmetric  $\text{CH}_3$  stretching, whereas the bands at  $2912\text{ cm}^{-1}$  and  $2844\text{ cm}^{-1}$  could be C–H stretching modes of  $\text{CH}_3$  or  $\text{CH}_2$  groups [55]. IR spectroscopy thus gives evidence of carbon enrichment in the pure cobalt catalyst, which was also confirmed by C, H analysis (Fig. S13), where carbon was found to be 30 wt % of the recovered catalyst. Additionally, a thermogravimetric analysis of the spent sample shows a drastic mass loss around  $300^\circ\text{C}$  of about 28 % of the cobalt catalyst (Fig. S14), which corresponds to the burn-off of the deposited coke. However, the stability of the catalytic performance of the cobalt catalyst was good over the 165 h of run time, despite the coke formation.

All copper-containing catalysts contained only small amounts of carbon and hydrogen, which can be assigned to carbonate groups or re-adsorbed water, as neither the IR spectra nor the TG analysis delivered clear further evidence for coke formation or burn-off. The TGA curves showed a mass gain due to metal oxidation rather than a mass loss due to burn-off of deposited hydrocarbons. This also confirms that the catalyst passivation was successful and substantial fraction of the catalyst have remained in the metallic state. These results show that the presence of copper strongly suppresses the formation of coke during HAS on the catalysts studied here. Such a promotion by copper was also observed by Cu–Ni or Cu–Co catalysts in other reaction systems [56–58]. To the best of our knowledge the promotion effect of copper on the coke suppression was not yet discussed in the context of higher alcohol synthesis.

## 4 Conclusion

The addition of copper prevents coke formation on cobalt catalysts and enhances the selectivity towards alcohols at temperatures below  $250^\circ\text{C}$  in Cu–Co/ZnAl<sub>2</sub>O<sub>4</sub> catalysts. Bi-metallic catalysts showed a clearly different behavior, which was beneficial for HAS, compared to the pure copper or cobalt catalysts. The XRPD data suggests a possible alloy formation of Cu and Co in the ccp phase, which would imply a close interaction of both metals. Relatively low pressure (20 bar) and temperatures above  $225^\circ\text{C}$  result in complete conversion at an *GHSV* of around  $2800\text{ h}^{-1}$  in a synthesis gas stream of a  $\text{H}_2:\text{CO}$  ratio of 4. Unfortunately, these process conditions were found not to result in an increase in the HAS activity of the catalysts. Compared to literature reports, the selectivity to higher alcohols of the studied catalysts was low at otherwise high activity. However, a copper content of already 12.5 at %, which is accompanied by a significant drop of the domain size of the ccp phase compared

to the pure cobalt catalyst, has a positive effect on the alcohol selectivity from CO hydrogenation and on the mitigation of coking. Nevertheless, the hydrocarbon selectivity was found to be always predominant in this hydrogen-rich synthesis gas.

Another important effect of copper was the facilitated reduction of the cobalt oxide. The activity of the pure copper catalyst was enhanced, and methanol formation was improved after a treatment in reducing gas at  $380^\circ\text{C}$ . These results demonstrated the necessity of higher temperatures to reach a completely activated state of this Cu/ZnAl<sub>2</sub>O<sub>4</sub> catalyst from a hydrotalcite precursor. The activation of the pure cobalt catalyst was also not complete prior to the catalytic experiment and proceeded after each temperature or pressure variation. Even though significant coke formation was found for this catalyst, it showed – just like the other hydrotalcite-derived catalysts studied here – a stable catalytic performance after it was fully activated up to 165 h on stream.

## Supporting Information

Supporting Information for this article can be found under DOI: <https://doi.org/10.1002/cite.202200171>. This section includes additional references to primary literature relevant for this research [59–70].

This work was supported by the Mercator Research Center Ruhr (MERCUR Pe-2018-0034). F.Ö. thanks the International Max Planck Research School RECHARGE for support. Prof. S. Schulz and Prof. M. Epple of the University of Duisburg-Essen are gratefully acknowledged for allocating access to their characterization facilities. Open access funding enabled and organized by Projekt DEAL.

## Symbols used

$a$	[Å]	Cell parameter
$c$	[Å]	Cell parameter
$D_{\text{Vol}}$	[nm]	Isotropic crystallite size (volume average)
<i>GHSV</i>	[h <sup>-1</sup> ]	Gas hourly space velocity
$\Delta_r H^\circ$	[kJ mol <sup>-1</sup> ]	Reaction enthalpy
$l$	[-]	Millersche indices (hkl) (unique designation of crystal faces)
$m$	[-]	Number
$n$	[mol]	Molar amount
$S$	[%]	Selectivity
$T$	[°C]	Temperature
$x$	[-]	Cu fraction based on Cu and Co
$X$	[%]	Conversion

## Greek letters

$\nu$	[-]	Vibration mode
$\theta$	[°]	Diffraction angle

## Abbreviations

ccp	Cubic closed package
DFT	Density functional theory
FTS	Fischer-Tropsch synthesis
GC	Gas chromatography
HAS	Higher alcohol synthesis
hcp	Hexagonal closed package
IR	Infrared
M <sup>2+</sup>	Divalent cation
M <sup>3+</sup>	Trivalent cation
MMO	Mixed metal oxide
n-C <sub>#</sub>	Linear hydrocarbon / alcohol with # carbon atoms
SMSI	Strong metal support interaction
TGA	Thermogravimetric analysis
TPR	Temperature programmed reduction
WGS	Water gas shift
XRPD	X-ray powder diffraction

## References

- V. R. Calderone, N. R. Shiju, D. C. Ferré, G. Rothenberg, *Green Chem.* **2011**, *13* (8), 1950–1959.
- V. Garcilaso et al., *Renewable Energy* **2019**, *132*, 1141–1150.
- K. G. Fang et al., *Catal. Today* **2009**, *147* (2), 133–138. DOI: <https://doi.org/10.1016/j.cattod.2009.01.038>
- H. Schulz, *Appl. Catal., A* **1999**, *186* (1), 3–12. DOI: [https://doi.org/10.1016/S0926-860X\(99\)00160-X](https://doi.org/10.1016/S0926-860X(99)00160-X)
- M. Martinelli et al., *Appl. Catal., A* **2020**, *608*, 117740. DOI: <https://doi.org/10.1016/j.apcata.2020.117740>
- H. Jahangiri et al., *Catal. Sci. Technol.* **2014**, *4* (8), 2210–2229. DOI: <https://doi.org/10.1039/C4CY00327F>
- A. Jess, P. Wasserscheid, *Chemical Technology: An Integral Textbook*, Wiley-VCH, Weinheim **2013**.
- P. Forzatti, E. Tronconi, I. Pasquon, *Catal. Rev.* **1991**, *33* (1–2), 109–168. DOI: <https://doi.org/10.1080/01614949108020298>
- K. Xiao et al., *Catal. Sci. Technol.* **2013**, *3* (6), 1591–1602. DOI: <https://doi.org/10.1039/c3cy00063j>
- J. Anton et al., *Top. Catal.* **2016**, *59* (15–16), 1361–1370. DOI: <https://doi.org/10.1007/s11244-016-0663-2>
- A. J. Medford et al., *Top. Catal.* **2014**, *57* (1), 135–142. DOI: <https://doi.org/10.1007/s11244-013-0169-0>
- A. Cao et al., *ACS Catal.* **2018**, *8* (11), 10148–10155. DOI: <https://doi.org/10.1021/acscatal.8b01596>
- V. Subramani, S. K. Gangwal, *Energy Fuels* **2008**, *22* (2), 814–839. DOI: <https://doi.org/10.1021/ef700411x>
- T. Nishizawa, K. Ishida, *Bull. Alloy Phase Diagrams* **1984**, *5* (2), 161–165. DOI: <https://doi.org/10.1007/BF02868953>
- G. Prieto et al., *Angew. Chem., Int. Ed.* **2014**, *53* (25), 6397–401. DOI: <https://doi.org/10.1002/anie.201402680>
- A. Cao et al., *RSC Adv.* **2015**, *5* (72), 58804–58812. DOI: <https://doi.org/10.1039/C5RA05190H>
- P. Courty, D. Durand, E. Freund, A. Sugier, *J. Mol. Catal.* **1982**, *17* (2), 241–254. DOI: [https://doi.org/10.1016/0304-5102\(82\)85035-9](https://doi.org/10.1016/0304-5102(82)85035-9)
- G. Behrendt et al., *ChemCatChem* **2022**, *14* (17), e202200299. DOI: <https://doi.org/10.1002/cctc.202200299>
- J. A. Dalmon, P. Chaumette, C. Mirodatos, *Catal. Today* **1992**, *15* (1), 101–127. DOI: [https://doi.org/10.1016/0920-5861\(92\)80124-6](https://doi.org/10.1016/0920-5861(92)80124-6)
- B. C. Enger et al., *J. Catal.* **2013**, *297*, 187–192. DOI: <https://doi.org/10.1016/j.jcat.2012.10.013>
- H. Wang et al., *J. Mol. Catal. A: Chem.* **2010**, *326* (1), 29–40. DOI: <https://doi.org/10.1016/j.molcata.2010.04.009>
- J. A. Singh et al., *ChemCatChem* **2019**, *11* (2), 799–809. DOI: <https://doi.org/10.1002/cctc.201801724>
- S. M. Auerbach, K. A. Carrado, P. K. Dutta, *Handbook of Layered Materials*, Taylor & Francis, London **2004**.
- K. Sun et al., *ChemCatChem* **2019**, *11* (11), 2695–2706. DOI: <https://doi.org/10.1002/cctc.201900096>
- F. Studt et al., *ChemCatChem* **2015**, *7* (7), 1105–1111. DOI: <https://doi.org/10.1002/cctc.201500123>
- I. C. t. Have et al., *Nat. Commun.* **2022**, *13* (1), 324. DOI: <https://doi.org/10.1038/s41467-022-27981-x>
- A. A. Mirzaei et al., *RSC Adv.* **2015**, *5* (115), 95287–95299. DOI: <https://doi.org/10.1039/C5RA13427G>
- E. van Steen, H. Schulz, *Appl. Catal., A* **1999**, *186* (1), 309–320. DOI: [https://doi.org/10.1016/S0926-860X\(99\)00151-9](https://doi.org/10.1016/S0926-860X(99)00151-9)
- J. Anton et al., *J. Catal.* **2016**, *335*, 175–186.
- K. Chakrapani et al., *ChemElectroChem* **2018**, *5* (1), 93–100. DOI: <https://doi.org/10.1002/celec.201700936>
- H. Rietveld, *Acta Crystallogr.* **1967**, *22* (1), 151–152.
- A. A. Coelho, *J. Appl. Crystallogr.* **2018**, *51* (1), 210–218.
- G. Pawley, *J. Appl. Crystallogr.* **1981**, *14* (6), 357–361.
- A. A. Coelho, J. S. Evans, J. W. Lewis, *J. Appl. Crystallogr.* **2016**, *49* (5), 1740–1749.
- M. Behrens, R. Schlogl, *Z. Anorg. Allg. Chem.* **2013**, *639* (15), 2683–2695. DOI: <https://doi.org/10.1002/zaac.201300356>
- J. Schumann et al., *Appl. Catal., A* **2016**, *516*, 117–126. DOI: <https://doi.org/10.1016/j.apcata.2016.01.037>
- L. Pandit et al., *ChemCatChem* **2021**, *13* (19), 4120–4132. DOI: <https://doi.org/10.1002/cctc.202100692>
- S. Kühl et al., *Chem. – Eur. J.* **2014**, *20* (13), 3782–3792. DOI: <https://doi.org/10.1002/chem.201302599>
- A. Tarasov, S. Kuhl, J. Schumann, M. Behrens, *High Temp. – High Pressures* **2013**, *42* (4), 377–386.
- P. Hazemann et al., *J. Catal.* **2021**, *397*, 1–12. DOI: <https://doi.org/10.1016/j.jcat.2021.03.005>
- G. Kwak et al., *Catal. Sci. Technol.* **2016**, *6* (12), 4594–4600. DOI: <https://doi.org/10.1039/C5CY01399B>
- R. Dalebout et al., *ACS Catal.* **2022**, *12*, 6628–6639.
- B. R. van den Berg et al., *Nat. Commun.* **2016**, *7*, 13057. DOI: <https://doi.org/10.1038/ncomms13057>
- M. Behrens et al., *Science* **2012**, *336* (6083), 893–897. DOI: <https://doi.org/10.1126/science.1219831>
- J. Popović et al., *Am. Mineral.* **2009**, *94* (5–6), 771–776.
- E. Owen, D. M. Jones, *Proc. Phys. Soc., London, Sect. B* **1954**, *67* (6), 456.
- Binary Alloy Phase Diagrams* (Ed: T. B. Massalski), 2nd ed., ASM International, Materials Park, OH **1990**, 1261–1263.
- F. Vincent, M. Figlarz, *C. R. Seances Acad. Sci., Ser. C* **1967**, *264* (15), 1270–1273.
- G. P. Vassiley, M. Jiang, *J. Phase Equilib. Diffus.* **2004**, *25* (3), 259–268.
- B. Eren et al., *J. Am. Chem. Soc.* **2018**, *140* (21), 6575–6581. DOI: <https://doi.org/10.1021/jacs.7b13621>
- N. E. Tsakoumis et al., *Appl. Catal., A* **2014**, *479*, 59–69. DOI: <https://doi.org/10.1016/j.apcata.2014.03.035>
- C. Göbel et al., *J. Catal.* **2020**, *383*, 33–41. DOI: <https://doi.org/10.1016/j.jcat.2020.01.004>

- [53] J. Anton, H. Ruland, S. Kaluza, M. Muhler, *Catal. Lett.* **2015**, *145* (7), 1374–1381. DOI: <https://doi.org/10.1007/s10562-015-1543-2>
- [54] L. P. A. F. Elst, S. Eijssbouts, A. D. van Langeveld, J. A. Moulijn, *J. Catal.* **2000**, *196* (1), 95–103. DOI: <https://doi.org/10.1006/jcat.2000.3011>
- [55] C. Leyva et al., *Catal. Today* **2014**, 220–222, 89–96. DOI: <https://doi.org/10.1016/j.cattod.2013.10.007>
- [56] A. Vizcaíno, A. Carrero, J. Calles, *Int. J. Hydrogen Energy* **2007**, *32* (10–11), 1450–1461.
- [57] D. Homsí et al., *Environ. Sci. Pollut. Res.* **2017**, *24* (11), 9907–9913. DOI: <https://doi.org/10.1007/s11356-016-7480-9>
- [58] F. S. Toniolo, R. N. S. H. Magalhães, C. A. C. Perez, M. Schmal, *Appl. Catal., B* **2012**, *117–118*, 156–166. DOI: <https://doi.org/10.1016/j.apcatb.2012.01.009>
- [59] J. T. Klopogge, R. L. Frost, *J. Solid State Chem.* **1999**, *146* (2), 506–515. DOI: <https://doi.org/10.1006/jssc.1999.8413>
- [60] S. M. Auerbach, K. A. Carrado, P. K. Dutta, *Handbook of Layered Materials*, Taylor & Francis, London **2004**.
- [61] J. T. Klopogge, D. Wharton, L. Hickey, R. L. Frost, *Am. Mineral.* **2002**, *87* (5–6), 623–629. DOI: <https://doi.org/10.2138/am-2002-5-604>
- [62] F. Rey, V. Fornés, J. M. Rojo, *J. Chem. Soc., Faraday Trans.* **1992**, *88* (15), 2233–2238.
- [63] W. Kagunya, R. Baddour-Hadjean, F. Kooli, W. Jones, *Chem. Phys.* **1998**, *236* (1), 225–234. DOI: [https://doi.org/10.1016/S0301-0104\(98\)00234-1](https://doi.org/10.1016/S0301-0104(98)00234-1)
- [64] R. N. Pease, H. S. Taylor, *J. Am. Chem. Soc.* **1921**, *43* (10), 2179–2188.
- [65] J. S. Lewis, *J. Chem. Soc.* **1932**, 820–826. DOI: <https://doi.org/10.1039/JR9320000820>
- [66] O. P. Tkachenko et al., *J. Phys. Chem. B* **2005**, *109* (44), 20979–20988. DOI: <https://doi.org/10.1021/jp054033i>
- [67] A. Alejandre et al., *Chem. Mater.* **1999**, *11* (4), 939–948. DOI: <https://doi.org/10.1021/cm980500f>
- [68] S. Velu et al., *J. Mater. Chem.* **2001**, *11* (8), 2049–2060. DOI: <https://doi.org/10.1039/B101599K>
- [69] L. Pandit et al., *ChemCatChem* **2021**, *13* (19), 4120–4132. DOI: <https://doi.org/10.1002/cctc.202100692>
- [70] C.-W. Tang, C.-B. Wang, S.-H. Chien, *Thermochim. Acta* **2008**, *473* (1), 68–73. DOI: <https://doi.org/10.1016/j.tca.2008.04.015>